Journal of Power Sources 270 (2014) 564–568

Contents lists available at ScienceDirect

Journal of Power Sources

journal homepage: www.elsevier.com/locate/jpowsour

Short communication

A novel electrochemical reconstruction in nickel oxide nanowalls on Ni foam and the fine electrochemical performance as anode for lithium ion batteries

Shibing Ni [a, b], Xiaohu Lv [a], Jianjun Ma [a], Xuelin Yang [a, b, *], Lulu Zhang [a, b]

[a] College of Materials and Chemical Engineering, Three Gorges University, 8 Daxue Road, Yichang, Hubei 443002, China
[b] Hubei Provincial Collaborative Innovation Center for New Energy Microgrid, Three Gorges University, China

HIGHLIGHTS

- We prepared NiO nanowalls/Ni composite architecture.
- The NiO/Ni anode exhibits high areal capacity and good cycle stability and rate capability.
- A novel electrochemical reconstruction in NiO/Ni was observed.

GRAPHICAL ABSTRACT

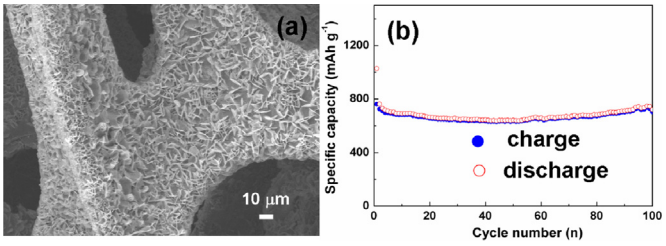

ARTICLE INFO

Article history:
Received 17 March 2014
Received in revised form
21 July 2014
Accepted 22 July 2014
Available online 30 July 2014

Keywords:
Electrochemical corrosion
Nickel oxide
Lithium ion battery
Electrochemical reconstruction

ABSTRACT

NiO nanowalls are directly grown on porous Ni foam via a facile electrochemical corrosion method and subsequent annealing, which show excellent cycle stability and rate capability as anode for lithium ion batteries. It delivers initial discharge and charge capacity of 1029 and 761 mAh g^{-1} at 0.15C, maintaining of 721 and 704 mAh g^{-1} after 100 cycles. After 60 cycles at various rates from 0.06 to 10C, the discharge capacity of the NiO/Ni can gradually restore when lowering the charge/discharge, finally arriving at 745 mAh g^{-1} after 30 cycles at 0.06C. The excellent electrochemical performance of the NiO/Ni electrode is relevant to a novel electrochemical reconstruction in cycling, which can be described as the initial formation of a large number of nanosized particles and the subsequent reassembly of these nanoparticles into a unique porous architecture.

1. Introduction

Lithium ion batteries are becoming not only the main power source in today's portable electronic devices but also the potential power sources of electric vehicles and hybrid electric vehicles. One of the key issues in the development of lithium ion batteries is the exploration and design of advanced electrode materials with higher capacity and better electrochemical performance.

NiO is a promising anode for high performance lithium ion batteries owing to its high theoretical capacity, low cost, environmental friendly and abundance [1]. However, it shows poor cycling performance because of its low electronic conductivity and structure destruction in cycling. Combining it with electric substrate has been testified to be an effective way to improve its electronic conductivity and structure stability, which is beneficial to improve the electrochemical performance of NiO [2]. Among them, Ni foam becomes an ideal electric substrate owing to its three dimensional porous architecture and big surface area. For example, NiO/Ni

* Corresponding author. College of Materials and Chemical Engineering, Three Gorges University, 8 Daxue Road, Yichang, Hubei 443002, China. Fax: +86 717 6397559.
E-mail addresses: shibingni07@gmail.com (S. Ni), xlyang@ctgu.edu.cn (X. Yang).

http://dx.doi.org/10.1016/j.jpowsour.2014.07.137
0378-7753/

electrodes were prepared via oxidizing Ni foam in air and chemical liquid deposition with subsequent annealing, which exhibit attractive electrochemical performance [3–5].

However, it is known that the electrochemical performance of film electrode is usually sensitive to the mass of active material. The less the active material is, the better the electrochemical performance of film electrode shows [3,4]. Thus improving the mass of active NiO in NiO/Ni without worsening the electrochemical performance is of great importance for the application of NiO/Ni in lithium ion batteries.

Here in this paper we report the preparation of high performance NiO/Ni anode via an electrochemical corrosion method, and the weight of NiO is distinctly increased via adding appropriate amount of H_2O_2. The fine electrochemical performance of the NiO/Ni is proposed to be relevant to a novel electrochemical reconstruction process, which leads to the formation of a new porous architecture in cycling.

2. Experiments

2.1. Sample preparation

Ni foam (100 PPI pore size, 380 g m^{-2} surface density, 1.5 mm thick) was purchased from Changsha Lyrun New Material corporation. In a typical procedure, Ni foam was firstly put into diluted hydrochloric acid ($HCl:H_2O = 1:10$) until the solution changes into pea green to eliminate the surface oxide layer. Then it was ultrasonically washed with distilled water to remove the rudimental Cl^-. The washed Ni foam was placed into a 50 ml teflonlined autoclave, distilled water and 0.6 ml H_2O_2 was subsequently added to 80% of its capacity. The autoclave was sealed and placed in an oven, heated at 120 °C for 24 h. After the reaction, the autoclave was cooled in air. The hydrothermal treated Ni foam was dried in an oven at 70 °C for 24 h, and then annealed in N_2 atmosphere at 300 °C for 5 h (heating rate of 3 °C min^{-1}). According to the reaction ($Ni(OH)_2 \rightarrow NiO + H_2O$), the weight of NiO can be estimated. $m_{NiO} = \Delta m \times 74.7/18$, where Δm is the weight difference of $Ni(OH)_2$/Ni before and after annealing in N_2 atmosphere.

2.2. Structure and morphology characterization

The structure and morphology of the resulting products were characterized by X-Ray powder diffraction (Rigaku Ultima IV Cu Kα radiation $\lambda = 1.5406$ Å), field-emission scanning electron microscopy (FE-SEM JSM 7500F, JEOL), and transmission electron microscopy (TEM, FEI, Tecnai G2 F30) equipped with selected area electron diffraction (SAED). The NiO/Ni electrode was cut into small pieces and ultrasonic treated in ethanol before TEM characterization. For characterizing the morphology and microstructure of the electrode after cycling test, the cycled cell was disassembled in air and the electrode was washed with ethanol and distilled water. For comparison, the cycled electrode was also disassembled in glove box (MIKROUNA, Super 1220/750, $H_2O < 1.0$ ppm, $O_2 < 1.0$ ppm) and washed by dimethyl carbonate.

2.3. Electrochemical characterization

For fabricating of lithium ion battery, the as-prepared NiO/Ni foam discs were dried at 120 °C for 24 h in vacuum. Coin-type cells (2025) of Li/1 M $LiPF_6$ in ethylene carbonate, dimethyl carbonate and diethyl carbonate (EC/DMC/DEC, 1:1:1 v/v/v)/NiO/Ni disc electrode with diameter of 14 mm were assembled in a glove box (MIKROUNA, Super 1220/750, $H_2O < 1.0$ ppm, $O_2 < 1.0$ ppm). A Celgard 2400 microporous polypropylene was used as the separator membrane. The cells were tested in the voltage range between 0.02 and 3 V with a multichannel battery test system (LAND CT2001A). The Cyclic voltammetry (CV) measurement of the electrodes was carried out on a CHI660C electrochemical workstation at a scan rate of 0.2 mV s^{-1} between 0 and 3 V.

3. Results and discussion

Fig. 1 is the XRD pattern of the as-prepared electrode. As seen, three typical diffraction peaks located at 44.4°, 51.7° and 76.4° correspond to Ni (111), (200) and (220) faces, respectively (JCPDS, No. 04-0850). Diffraction peaks other than those of Ni, which located at 37.5°, 43.4° and 63.1°, respectively, can be attributed to the (101), (012) and (110) faces of NiO (JCPDS, No. 44-1159). (The formation process see ESI†, Fig. S1 and Fig. S2).

The morphology and microstructure of the NiO/Ni electrode were studied by SEM and TEM. Fig. 2(a) is a low magnification SEM image of the NiO/Ni, which exhibits nanowall-like morphology, consisting of a large number of interlaced nanoflakes. High magnification SEM image of the NiO/Ni is shown in Fig. 2(b). As seen, the mean size and mean thickness of these nanoflakes are about 6 μm and 100 nm, respectively. As shown in a TEM image in Fig. 2(c), the obtained NiO nanoflakes are composed of a large number of small particles with mean size about 20 nm. The inset of Fig. 2(c) is a SAED pattern of the NiO nanoflakes, from which clear diffraction spots that distribute in rings can be observed, suggesting the obtained NiO nanoflakes are well crystallized and polycrystalline. Fig. 2(d) is a HR-TEM image of the NiO nanoflakes, which shows clear crystal grain boundaries and lattice fringes, illustrating that the NiO nanoflakes are polycrystalline. As seen, the interplanar spacing of a single particle is about 0.24 nm, which corresponds to the (101) plane of the hexagonal NiO.

The galvanostatic test of the NiO/Ni electrode was carried out in the potential window 0.02–3.00 V at a charge/discharge rate of 0.15C (1C means accomplishing discharge or charge in an hour, 0.2 mA cm^{-2}). As shown in Fig. 3(a), the charge and discharge curves of the NiO/Ni are similar to those in literature [2–5]. The initial discharge capacity of the NiO/Ni is 1028 mAh g^{-1}, higher than the initial charge capacity of 760 mAh g^{-1}, which is due to the irreversible consumption of lithium ions during the formation of solid electrolyte interface (SEI) [3–5]. As seen, the discharge capacity for the 2nd and 3rd cycle is 760 and 730 mAh g^{-1}, respectively, which attenuates slightly along with the increasing of cycle number in the first few cycles and then gradually reaches stable value, being 721 mAh g^{-1} for the 100th cycle. The cycle stability of

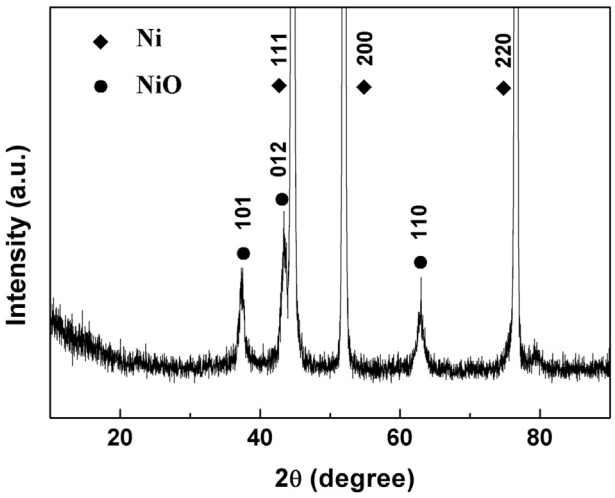

Fig. 1. XRD pattern of the prepared sample.

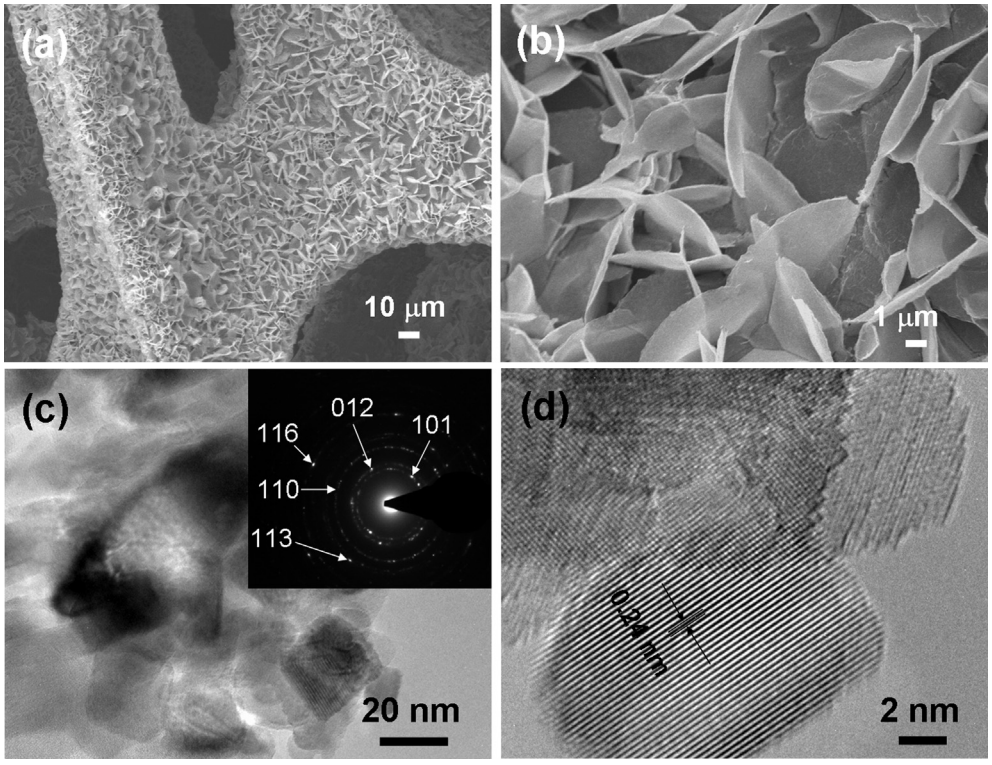

Fig. 2. SEM image with low (a) and high (b) magnification, TEM (c) and HR-TEM (d) images of the as-prepared NiO/Ni electrode. The inset of (c) is the corresponding SAED pattern.

the NiO/Ni electrode is much improved than that of NiO reported in literature [6–9], and the areal capacity of the NiO/Ni electrode is higher than that of $Ni(OH)_2$/Ni, NiO/Ni, Fe_3O_4/Cu and Cu_xO/Cu ($x = 1, 2$) film electrodes (areal capacity see ESI†, Fig. S3) [2,10–13].

The high areal capacity of the NiO/Ni electrode is relevant to the presence of H_2O_2, which promotes the electrochemical corrosion process and leads to the increase of active NiO on Ni foam (areal capacity of NiO/Ni obtained without H_2O_2 see ESI†, Fig. S4). Fig. 3(b)

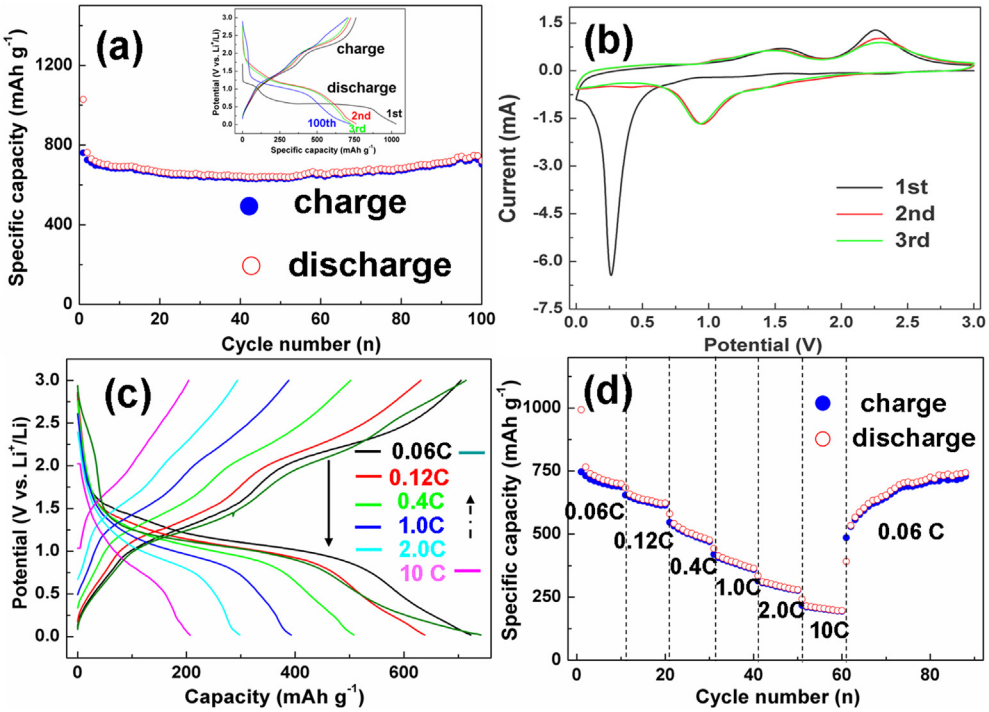

Fig. 3. Electrochemical performance of the NiO/Ni electrode. (a) Capacity retention of the galvanostatic test runs at a rate of 0.15C. The inset shows the initial three and 100th charge and discharge curves. (b) Cyclic voltammograms at a scan rate of 0.2 mV s^{-1}. (c) Representative charge and discharge voltage profiles at various rates. (d) Capacity retention at various rates.

is the cyclic voltammetric (CV) curves of the NiO/Ni electrode tested over a voltage range from 0 to 3.0 V at a scan rate of 0.2 mV s^{-1}. As seen, the profiles of CV curves of the 2nd and 3rd cycle are similar, whereas an obvious difference between the first and subsequent two cycles is found. In the 1st cathodic scan, a strong reduction peak at around 0.26 V is observed, which is attributed to the formation of SEI and Ni [3–5]. The location of the reduction peak is smaller than the voltage plateau in the first discharge curve, which can be ascribed to polarization. In CV measurement, the location of reduction peaks is relevant to scan rate. As shown in previous study, the initial reduction peak for NiO/Ni locates at 0.57, 0.46 and 0.22 V at a scan rate of 0.058, 0.1 and 0.2 mV s^{-1}, respectively [2,4,5]. The strong reduction peak shifts to 0.94 V in the 2nd cathodic scan owing to the activation of electrode [3]. In the subsequent cycles, the two oxidation peaks of NiO, located at about 1.54 and 2.29 V, could be attributed to the partial decomposition of SEI and the formation of NiO, respectively [2–4]. Fig. 3(c) shows the discharge and charge curves of the NiO/Ni electrode at various charge/discharge rates. Along with the increasing of charge/discharge rate, the discharge potential decreases and the charge potential increases due to kinetic effects of the material, rendering higher overpotential [4,5]. Meanwhile, the charge and discharge capacity decrease along with the increasing of charge/discharge rate. As shown in Fig. 3(d), the 5th-cycle discharge capacity is 723, 699, 638, 508, 298 and 207 mAh g^{-1} at 0.06, 0.12, 0.4, 1.0, 2.0 and 10C, respectively. The phenomena can be understood as a polarization: along with the increasing of charge/discharge rate, the electrochemical reactions between electrolyte and active materials become insufficient. The higher the charge/discharge rate the more insufficient the electrochemical reactions, which results in capacity loss along with the increasing of charge/discharge rate. After that, the discharge capacity can restore gradually when lowering the charge/discharge rate to 0.06C, showing discharge capacity of 745 mAh g^{-1} after 30 cycles at 0.06C.

According to the reversible electrochemical reaction for metal oxides ($M_xO_y + 2ye^- + 2yLi^+ \rightleftharpoons xM + yLi_2O$), one can deduce that nanosized metal will generate in discharge due to a recrystallization process, which can be described as electrochemical activation [3,14]. These nanosized Ni will reassemble into secondary architecture to reduce the surface free energy. Under normal reaction condition, they will prefer to aggregate, which can be described as electrochemical sintering [3,5]. However, they can also reassemble into new favorable architectures in cycling if they possess a special original architecture, which can be described as electrochemical reconstruction [14]. In any case, the original morphology and microstructure of the NiO/Ni will change in cycling. SEM and TEM were employed to study the morphology variation of the NiO/Ni electrode. Fig. 4(a) is a low magnification SEM image of the cycled NiO/Ni electrode, from which porous architecture that differs much from the original morphology can be observed, suggesting a reconstruction process in cycling. For further studying the microstructure of the cycled NiO/Ni, a high magnification SEM image is shown in Fig. 4(b). As seen, the porous architecture originates from the assembly of a large number of nanosized particles, among which many holes with size several tens of nanometers exhibit. Fig. 4(c) is a TEM image of the cycled NiO, which shows a large number of nanoparticles with mean size less than 10 nm. The inset of Fig. 4(c) is a SAED pattern of the cycled NiO, from which clear diffraction rings correspond to the (012) and (113) planes of NiO can be observed, indicating polycrystalline characteristic of the cycled NiO. Fig. 4(d) is a HR-TEM image of the cycled NiO, from which clear boundaries of crystal grain and lattice

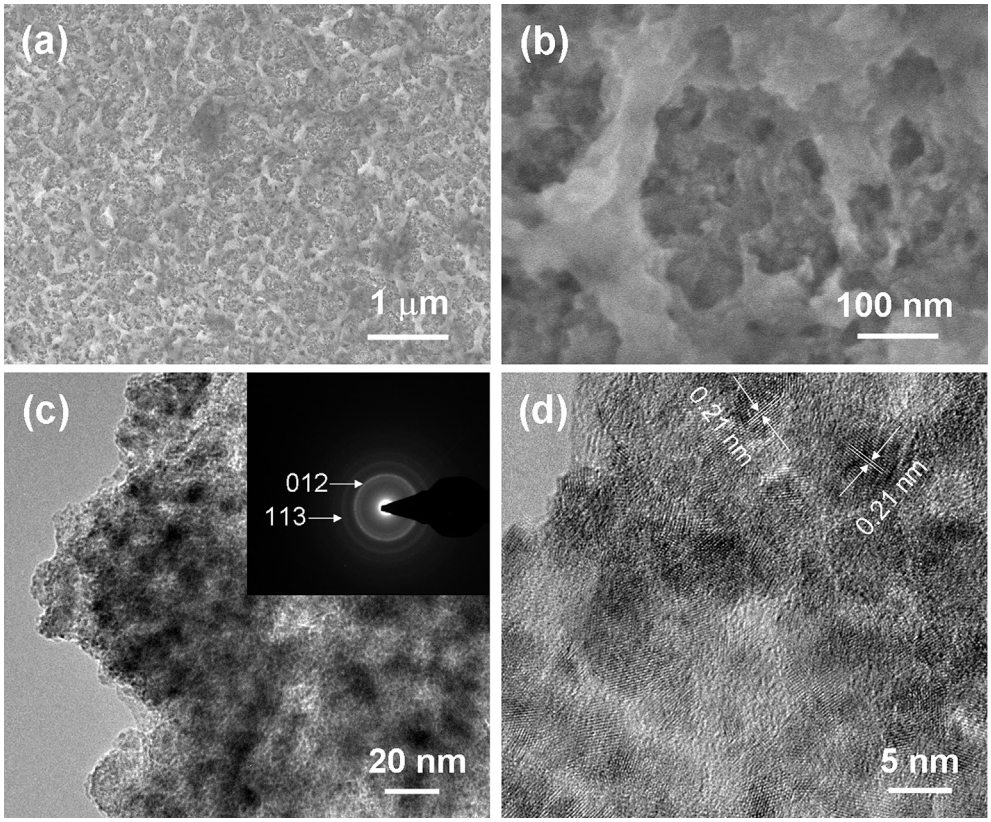

Fig. 4. SEM images of the NiO/Ni electrode after 10 cycles with charge state that disassembles in air and washed by ethanol and distilled water with low (a) and high (b) magnification. TEM (c) and HR-TEM (d) image of the cycled NiO/Ni electrode. The inset of (c) is the corresponding SAED pattern.

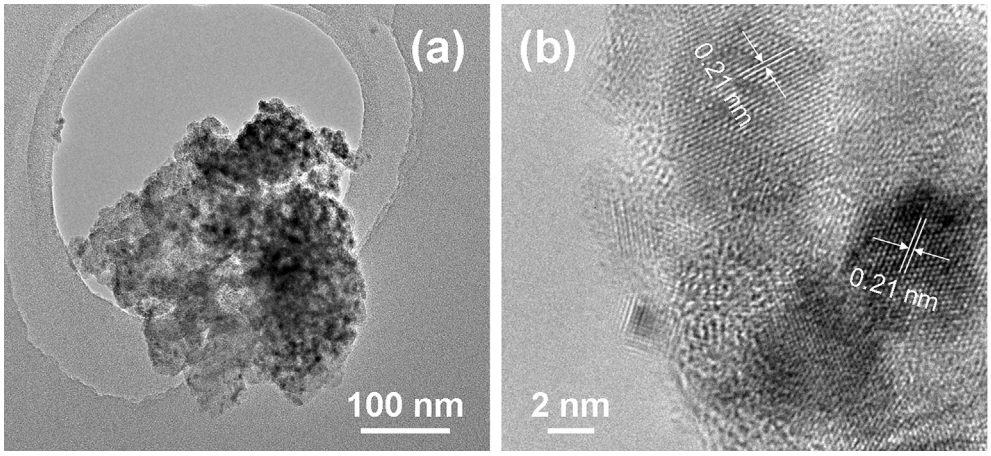

Fig. 5. SEM images of the NiO/Ni electrode after 10 cycles with charge state that disassembles in glove box and washed by DMC with low (a) and high (b) magnification.

fringes can be observed, illustrating the cycled NiO is polycrystalline. As seen, the interplanar spacing is about 0.21 nm, which corresponds to the (012) plane of hexagonal NiO. Such observations in SEM and TEM can be described as the electrochemical activation and electrochemical reconstruction, which accompanies by the initial formation of a large number of nanosized particles and subsequent reassembly of these nanoparticles into new porous architecture. The newly formed porous architecture is beneficial to improve the reaction kinetics and the structure stability of the NiO/Ni electrode, leading to good electrochemical performance. As we know, much research work has demonstrated that the electrochemical performance of redox reaction type anodes was distinctly affected by the original morphology of electrode material [4,15–17]. However, we want to emphasize it is the secondary morphology that forms in cycling shows direct relationship with the electrochemical performance of these anodes. The secondary morphology was determined by both the original morphology and architecture of the electrode and the electrochemical process. Herein we propose that the fine electrical contact between NiO and Ni, the nanowall-like morphology of NiO, and the porous architecture of the NiO/Ni can facilitate the electrochemical reaction kinetics and accommodate the volume variation, which induce the reconstruction process and result in the formation of a new porous architecture in cycling, leading to excellent electrochemical performance.

For comparison, the cycled cell was also disassembled in glove box, and the electrode was washed by DMC and naturally dried in the glove box. After that, the electrode was transferred to air atmosphere for the preparation of TEM sample. Fig. 5(a) is a TEM image of the cycled NiO, which consists of a large number of nanoparticles. A HR-TEM image of the cycled NiO is shown in Fig. 5(b), which exhibits clear lattice fringes with interplanar spacing about 0.21 nm, corresponding to the (012) plane of hexagonal NiO. In addition, clear boundaries of the lattice fringes demonstrate the polycrystalline characteristic of the cycled NiO. The observations are in accordance with those of the sample washed by ethanol and distilled water in air atmosphere.

4. Conclusions

In summary, NiO nanowalls on Ni foam were prepared by an electrochemical corrosion and subsequent annealing treatment, which shows excellent electrochemical performance as anode for lithium ion battery. The electrochemical performance was proposed to be relevant to the formation of porous architecture in charge/discharge test owing to a novel electrochemical reconstruction. The uniform porous architecture of the NiO/Ni electrode and the favorable morphology variation in cycling demonstrate great potential of the obtained NiO/Ni for further constructing new advanced composite electrodes.

Acknowledgment

We gratefully acknowledge the financial support from Natural Science Foundation of China (NSFC, 51272128, 51302152, 51302153). Moreover, the authors are grateful to Dr. Jianlin Li at Three Gorges University for his kind support to our research.

Appendix A. Supplementary data

Supplementary data related to this article can be found at http://dx.doi.org/10.1016/j.jpowsour.2014.07.137.

References

[1] P. Poizot, S. Laruelle, S. Grugeon, L. Dupont, J.M. Tarascon, Nature 407 (2000) 496–499.
[2] B. Varghese, M.V. Reddy, Z. .Yanwu, C.S. Lit, T.C. Hoong, G.V.S. Rao, B.V.R. Chowdari, A.T.S. Wee, C.T. Lim, C.H. Sow, Chem. Mater. 20 (2008) 3360–3367.
[3] C. Wang, D. Wang, Q. Wang, H. Chen, J. Power Sources 195 (2010) 7432–7437.
[4] X.H. Wang, X.W. Li, X.L. Sun, F. Li, Q.M. Liu, Q. Wang, D.Y. He, J. Mater. Chem. 21 (2011) 3571–3573.
[5] S.B. Ni, T. Li, X.H. Lv, X.L. Yang, L.L. Zhang, Electrochim. Acta 91 (2013) 267–274.
[6] X.H. Huang, J.P. Tu, X.H. Xia, X.L. Wang, J.Y. Xiang, L. Zhang, Y. Zhou, J. Power Sources 188 (2009) 588–591.
[7] X.H. Huang, J.P. Tu, X.H. Xia, X.L. Wang, J.Y. Xiang, Electrochem. Commun. 10 (2008) 1288–1290.
[8] G.P. Kim, S. Park, I. Nam, J. Park, J. Yi, J. Power Sources 237 (2013) 172–177.
[9] X.G. Liu, S.W. Or, C.G. Jin, Y.H. Lv, C. Feng, Y.P. Sun, Carbon 60 (2013) 215–260.
[10] S.B. Ni, X.H. Lv, T. Li, X.L. Yang, L.L. Zhang, J. Mater. Chem. A 1 (2013) 1544–1547.
[11] P.L. Taberna, S. Mitra, P. Poizot, P. Simon, J.M. Tarascon, Nat. Mater. 5 (2006) 567–573.
[12] H.N. Duan, J. Gnanaraj, X.P. Chen, B.Q. Li, J.Y. Liang, J. Power Sources 185 (2008) 512–518.
[13] S.B. Ni, X.H. Lv, T. Li, X.L. Yang, L.L. Zhang, Electrochim. Acta 109 (2013) 419–425.
[14] S.B. Ni, X.H. Lv, T. Li, X.L. Yang, L.L. Zhang, Y. Ren, Electrochim. Acta 96 (2013) 253–260.
[15] H. Wu, M. Xu, H.Y. Wu, J.J. Xu, Y.L. Wang, Z. Peng, G.F. Zheng, J. Mater. Chem. 22 (2012) 19821–19825.
[16] S.Q. Wang, J.Y. Zhang, C.H. Chen, J. Power Sources 195 (2010) 5379–5381.
[17] J.Y. Xiang, J.P. Tu, L. Zhang, Y. Zhou, X.L. Wang, S.J. Shi, J. Power Sources 195 (2010) 313–319.